The Astrophysical Journal, 757:139 (8pp), 2012 October 1 doi:10.1088/0004-637X/757/2/139

AN ULTRAVIOLET ULTRA-LUMINOUS LYMAN BREAK GALAXY AT $Z = 2.78$ IN NDWFS BOÖTES FIELD*,†,‡

Fuyan Bian[1], Xiaohui Fan[1], Linhua Jiang[1], Arjun Dey[2], Richard F. Green[3], Roberto Maiolino[4,5], Fabian Walter[6], Ian McGreer[1], Ran Wang[1], and Yen-Ting Lin[7,8]
[1] Steward Observatory, University of Arizona, 933 N. Cherry Avenue, Tucson, AZ 85721, USA
[2] National Optical Astronomy Observatory, 950 North Cherry Avenue, Tucson, AZ 85719, USA
[3] Large Binocular Telescope Observatory, University of Arizona, 933 N. Cherry Avenue, Tucson, AZ 85721, USA
[4] INAF Osservatorio Astronomico di Roma Via di Frascati 33, I-00040 Monte Porzio Catone, Italy
[5] Cavendish Laboratory, University of Cambridge, 19 J. J. Thomson Avenue, Cambridge, CB3 0HE, UK
[6] Max-Planck-Institut für Astronomie, Königstuhl 17, D-69117 Heidelberg, Germany
[7] Institute of Astronomy and Astrophysics, Academia Sinica, Taipei, Taiwan
[8] Institute for the Physics and Mathematics of the Universe, Todai Institutes for Advanced Study, The University of Tokyo, Kashiwa, Chiba, Japan
Received 2011 October 31; accepted 2012 July 31; published 2012 September 12

ABSTRACT

We present one of the most ultraviolet (UV) luminous Lyman break galaxies (LBGs; J1432+3358) at $z = 2.78$, discovered in the NOAO Deep Wide-Field Survey Boötes field. The *R*-band magnitude of J1432+3358 is 22.29 AB, more than two magnitudes brighter than typical L^* LBGs at this redshift. The deep *z*-band image reveals two components of J1432+3358 separated by 1.″0 with a flux ratio of 3:1. The high signal-to-noise ratio rest-frame UV spectrum shows Lyα emission line and interstellar medium absorption lines. The absence of N v and C iv emission lines, and the non-detection in X-ray and radio wavelengths and mid-infrared (MIR) colors indicates weak or no active galactic nuclei (<10%) in this galaxy. The galaxy shows a broader line profile, with a FWHM of about 1000 km s^{-1} and a larger outflow velocity (≈500 km s^{-1}) than those of typical $z \sim 3$ LBGs. The physical properties are derived by fitting the spectral energy distribution (SED) with stellar synthesis models. The dust extinction, $E(B-V) = 0.12$, is similar to that in normal LBGs. The star formation rates (SFRs) derived from the SED fitting and the dust-corrected UV flux are consistent with each other, ∼300 $M_\odot$ yr^{-1}, and the stellar mass is $(1.3 \pm 0.3) \times 10^{11}\ M_\odot$. The SFR and stellar mass in J1432+3358 are about an order of magnitude higher than those in normal LBGs. The SED-fitting results support that J1432+3358 has a continuous star formation history, with a star formation episode of 6.3×10^8 yr. The morphology of J1432+3358 and its physical properties suggest that J1432+3358 is in an early phase of a 3:1 merger process. The unique properties and the low space number density (∼10^{-7} Mpc^{-3}) are consistent with the interpretation that such galaxies are either found in a short unobscured phase of the star formation or that a small fraction of intensive star-forming galaxies are unobscured.

Key words: galaxies: high-redshift – galaxies: individual (J1432+3358) – galaxies: star formation

Online-only material: color figures

1. INTRODUCTION

Over the last decade, the dropout method (the Lyman break technique), which uses the fact that little flux is emitted blueward of the Lyman limit (912 Å), has been fundamental in searching for high-redshift star-forming galaxies (e.g., Steidel et al. 1996). Spectroscopic follow-up observations show that the efficiency of this method is high (e.g., Steidel et al. 2003, 2004). Large samples of Lyman break galaxies (LBGs) from $z \sim 2$ up to $z \sim 10$ have been established (e.g., Bouwens et al. 2008, 2011). These samples of LBGs provide crucial information on determining the cosmic star formation history (e.g., Madau et al. 1996; Lilly et al. 1996; Cowie et al. 1996), mapping the growth of large-scale structures (e.g., Adelberger et al. 1998; Giavalisco et al. 1998; Lee et al. 2006, 2009), and studying the properties of the dark matter halos which host the LBGs.

Optical and near-infrared (NIR) photometric and spectroscopic observations of these galaxies reveal the properties of the UV-selected galaxies at $z \sim 2$–3. The median stellar mass of the $z \sim 3$ LBGs is about $2.4 \times 10^{10}\ M_\odot$ (e.g., Shapley et al. 2001), and the mean star formation rate (SFR) derived from the Hα and UV luminosity is about 30 $M_\odot$ yr^{-1} (e.g., Erb et al. 2006b). The median dust extinction ($E(B-V)$) is around 0.15 (e.g., Shapley et al. 2001). The $z \sim 2$–3 LBGs show compact morphologies (half-light radii, $r_e < 0.''5$) in *Hubble Space Telescope* (*HST*) images (e.g., Giavalisco 1998).

However, most of optical/NIR surveys for high-redshift galaxies are deep field surveys with a survey area of less than 1 deg^2. Thus far, the largest $z \sim 2$–3 LBGs survey with spectroscopic redshifts only covers a total area of around 1 deg^2 with >2000 spectroscopic redshifts (e.g., Steidel et al. 2003; Reddy & Steidel 2009). Due to the small survey volume,

* Based on observations obtained at the Gemini Observatory, which is operated by the Association of Universities for Research in Astronomy, Inc., under a cooperative agreement with the NSF on behalf of the Gemini partnership: the National Science Foundation (United States), the Science and Technology Facilities Council (United Kingdom), the National Research Council (Canada), CONICYT (Chile), the Australian Research Council (Australia), Ministério da Ciência, Tecnologia e Inovação (Brazil), and Ministerio de Ciencia, Tecnología e Innovación Productiva (Argentina).

† Based on data acquired using the Large Binocular Telescope (LBT). The LBT is an international collaboration among institutions in the United States, Italy, and Germany. LBT Corporation partners are: The University of Arizona on behalf of the Arizona university system; Istituto Nazionale di Astrofisica, Italy; LBT Beteiligungsgesellschaft, Germany, representing the Max-Planck Society, the Astrophysical Institute Potsdam, and Heidelberg University; The Ohio State University, and The Research Corporation, on behalf of The University of Notre Dame, University of Minnesota, and University of Virginia.

‡ Based on (in part) data collected at Subaru Telescope, which is operated by the National Astronomical Observatory of Japan.

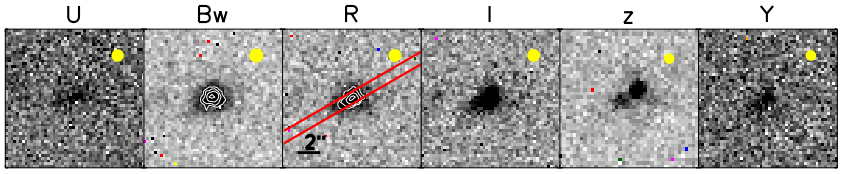

Figure 1. *U*-, B_W-, *R*-, *I*-, *z*-, and *Y*-band images of J1432+3358. A contour plot is also shown in B_W- and *R*-band images. The yellow filled circles represent the size of point-spread functions in each image. The typical image qualities for *U*-, B_W-, *R*-, *I*-, *z*-, and *Y*-band images are 1.″0, 1.″3, 1.″2, 1.″2, 0.″5, and 0.″6, respectively. The slit position and orientation are also shown in the *R*-band image.

(A color version of this figure is available in the online journal.)

combined with the rapid decline of the galaxy luminosity function at the bright end, these surveys are not suited to reveal the most luminous and most massive systems; previous studies have focused on LBGs with luminosities of L^* or sub-L^* ($r > 24.5$). A sample of bright LBGs was discovered in the Sloan Digital Sky Survey (SDSS); however, *HST* follow-up observations show that these galaxies are unresolved point sources, indicating that these objects are quasars rather than galaxies (Bentz et al. 2008). To date, only one unlensed LBG at $z \sim 3$ with an *R*-band magnitude brighter than 22.5 has been found (Cooke et al. 2008). The nature and properties of this type of galaxy are still unknown, so it is important to build up a sample of these UV ultra-luminous galaxies and perform detailed follow-up observations on them.

Finding UV ultra-luminous $z \sim 2$–3 galaxies requires wide-field surveys with deep, multi-color broadband images. In this paper, we report a UV ultra-luminous LBG, J1432+3358, with $R_{AB} = 22.29$ at $z = 2.78$ discovered in the NOAO Deep Wide Field Survey (NDWFS) Boötes field. Throughout this paper, we adopt $\Omega_m = 0.3, \Omega_\Lambda = 0.7$, and $H = 70\,\mathrm{km\,s^{-1}\,Mpc^{-1}}$ (Spergel et al. 2007). All the magnitudes are AB magnitudes.

2. OBSERVATIONS

In 2008 and 2009, we carried out deep *U*- and *Y*-band imaging of the 9 deg^2 NDWFS Boötes field (Jannuzi & Dey 1999). Our survey used the 2 × 8.4 m Large Binocular Telescope (LBT; Hill et al. 2010) equipped with two prime focus Large Binocular Cameras (Giallongo et al. 2008). This new LBT survey builds on the available unique multi-wavelength data of the NDWFS Boötes field and fills in two critical wavelength gaps at 3500 Å and 1 μm with the *U* and *Y* bands. The deep *U*-band images (25.2 AB magnitude with 5σ detection), together with the existing B_W- and *R*-band images taken with the Mosaic CCD camera on the Kitt Peak 4 m Mayall telescope, allow us to search for star-forming galaxies at $z \sim 3$ using the *U*-dropout technique, and a total of 15,000 LBG candidates are selected based on the $U - B_W$ and $B_W - R$ color–color diagram, with the selection criterion being

$$\begin{aligned} U - B_W &> 1.0, \\ B_W - R &< 1.9, \\ B_W - R &< U - B_W - 0.1, \\ R &< 25.0. \end{aligned} \quad (1)$$

The typical image quality in the *R* band is 1″ and thus cannot resolve typical LBGs. Nevertheless, the large survey area allows us to select and study the most UV luminous LBGs at $z \sim 3$ with $R < 22.5$ ($L > 7L^*$ at $z \sim 3$).

Spectroscopic follow-up observations of 12 of the bright LBG candidates were obtained using the blue channel spectrograph onboard the 6.5 m Multiple Mirror Telescope (MMT) on 2010 April 15. Typically, 20–40 minute exposures were taken for each candidate. The wavelength coverage is 4000–7500 Å. Out of 12 candidates, 1 was confirmed as a UV ultra-luminous LBG (J1432+3358) at $z = 2.78$, and the coordinates of this galaxy are R.A. = $14^h32^m21\overset{s}{.}84$ and decl. = 33°58′18.″2, J2000. The remaining 11 candidates are all quasars in the redshift range of $2 < z < 3$. All of these quasars show broad Lyα, N v, and C iv emission lines and they are all point sources.

A high signal-to-noise ratio (S/N) spectrum of J1432+3358 was obtained with the 8.2 m Gemini-N telescope and GMOS instrument on 2011 March 9 and 10 (Program ID: GN-2011-C-5). The sky was clear and the resulting image quality was 0.″6–0.″7. The total exposure time was 4 hr and was divided into 8 30 minute individual exposures. The slit width was 1″. The B600-G5307 grating was used, and two central wavelengths of 5200 Å and 5300 Å were used to fill the gaps between different CCD chips. The wavelength coverage was from 4000 Å to 6500 Å, and the spectral resolution ($R = \lambda/\delta\lambda$) is 850. The airmass of the object during the observing was about 1.05, and thus we did not use the parallactic angle. The slit oriented in position angle (P.A.) = −60°(300°), which was roughly along the galaxy extended direction (Figure 1). The spectrophotometric standard G191-B2B was observed for flux calibration, and a CuAr arc lamp was used for wavelength calibration. The spectra were reduced and calibrated using the standard Gemini IRAF package. The final spectrum has been smoothed by 4 Å. The S/N per spectral element (∼4 Å) is 8–10.

MIR photometry of J1432+3358 was obtained by the Spitzer Deep Wide-Field Survey (Ashby et al. 2009). In addition, an *H*-band image with 1 hr exposure was obtained using the SWIRC on 6.5 m MMT on 2012 January 5. We also obtained a deep *z*-band image from the Subaru Boötes field survey (BoötesZ Survey; Y. Lin et al. 2012, in preparation). The image quality of the *z*-band image is 0.″5. The total magnitudes of J1432+3358 are measured with SExtractor (Bertin & Arnouts 1996), and are listed in Table 1.

3. RESULTS

3.1. Lensed or Unlensed?

In the last decade, a sample of bright lensed high-redshift galaxies has been established through systematic searches toward galaxy clusters (e.g., Mehlert et al. 2001; Sand et al. 2005) and red galaxies in the SDSS images (e.g., Smail et al. 2007; Allam et al. 2007; Diehl et al. 2009; Lin et al. 2009). It is crucial to determine whether or not J1432+3358 is lensed. Studies suggest that the total fraction of high-redshift galaxies and quasars that are lensed is small (e.g., Turner et al. 1984; Jain & Lima 2011), but the lensing contribution becomes larger with increasing brightness. Jain & Lima (2011) find that the lensing contribution becomes significant when $L > 10L^*$, and about

Table 1
Magnitude and Morphological Properties of J1432+3358

Filter	Magnitude[a]	r_e[b]	n[c]	b/a[d]	θ[e]	χ^2/ν[f]
U	24.35 ± 0.13	...	...	...	...	...
B_W	23.26 ± 0.02	0.73 ± 0.20	3.10 ± 0.77	0.49 ± 0.05	-73.17 ± 3.75	1.310
R	22.29 ± 0.03	0.89 ± 0.04	1.23 ± 0.27	0.45 ± 0.04	-63.81 ± 2.84	1.078
I	22.20 ± 0.03	0.82 ± 0.05	1.37 ± 0.37	0.38 ± 0.05	-55.04 ± 3.05	1.104
z	22.13 ± 0.03	...	...	...	...	...
$z(a)$[g]	22.62 ± 0.04[h]	0.26 ± 0.03	4	0.69 ± 0.08	14.04 ± 13.21	1.168
$z(b)$[i]	23.71 ± 0.07[h]	0.21 ± 0.03	1	0.67 ± 0.14	82.43 ± 19.12	1.168
Y	22.19 ± 0.09	...	...	...	...	...
H	21.54 ± 0.36	...	...	...	...	...
IRAC1	20.88 ± 0.06	...	...	...	...	...
IRAC2	20.66 ± 0.07	...	...	...	...	...
IRAC3	20.69 ± 0.37	...	...	...	...	...
IRAC4	20.42 ± 0.33	...	...	...	...	...

Notes.
[a] Total AB magnitude from SExtractor.
[b] Effective radius ($''$) from the GALFIT fitting.
[c] Sérsic index from the GALFIT fitting.
[d] The ratio of minor axis (b) and major axis (a) from the GALFIT fitting.
[e] The position angle from the GALFIT fitting.
[f] The reduced χ^2 from the GALFIT fitting.
[g] The GALFIT fitting results of the brighter components in z-band image.
[h] The magnitude is from the GALFIT fitting.
[i] The GALFIT fitting results of the fainter components in z-band image.

one-third to one-half of the LBGs with $L = 7L^*$ are lensed galaxies (van der Burg et al. 2010).

The structure of J1432+3358 is well resolved by the ground-based imaging observations. The broadband U-, B_W-, R-, I-, z-, and Y-band images (Figure 1) of J1432+3358 show extended morphology. The deep multi-band images show that there is no foreground lensing galaxy and that the morphology of the galaxy is also consistent with being unlensed. Especially in the deep Subaru z-band image with an image quality of $0\farcs5$, J1432+3356 is revolved into two components, and the separation of these two parts is by $1\farcs0$ (7.8 kpc). These two components do not show the stretched arc structures at the resolution of the image. Furthermore, the central wavelengths of Lyα emission from these two components have a small offset (237 ± 23 km s^{-1}) and the Lyα flux ratio of these two components is not consistent with the continuum flux ratio of these two components (see details in Section 3.3). Meanwhile, the spectrum of J1432+3358 does not show any other redshift systems that could be from the lensing galaxy. Therefore, we conclude that J1432+3358 is not a lensed galaxy.

3.2. Morphology

The deep z-band image reveals two components in J1432+3358. We use GALFIT (Peng et al. 2002) to fit the light distribution of these two components with either exponential disk or DeVaucouleurs profiles. We find that the DeVaucouleurs profile is better to fit the brighter component and the exponential disk is better to fit the fainter component. The effective radii are $0\farcs26 \pm 0\farcs03$ and $0\farcs21 \pm 0\farcs03$, respectively, which correspond to about 2.0 kpc in physical size. This size is comparable to the typical size of LBGs at $z \sim 3$ (e.g., Ferguson et al. 2004). The distance between these two components is about $1\farcs0$, which is about 7.8 kpc. The brightness ratio between these two components in J1432+3358 is 3–1. Assuming a simple relation between luminosity and stellar mass, the mass ratio of the two components is also 3–1, implying that it is a 3:1 merger. These two components are barely resolved by the z-band image. Further high-resolution *HST* follow-up imaging observations will help us to fit the systems more accurately and to reveal a more detailed structure of this galaxy.

The morphology of J1432+3358 in the B_W-band image and that in the R- and I-band images looks different (Figure 1). To characterize the morphology in these bands, we use GALFIT to model the galaxy light distribution in the B_W-, R-, and I-band images of J1432+3358. The Sérsic profile (Sérsic 1963) is used to fit the light profile of J1432+3358. The GALFIT fitting results are listed in Table 1. The R- and I-band morphologies of J1432+3358 can be well fit by a disk-like profile with Sérsic index $n \approx 1.3$, while the Sérsic index is about 3.10 for the morphology in the B_W-band image, which is much larger than that in the R- and I-band images (Table 1). Furthermore, the galaxy light distribution in the B_W-band image cannot be well fitted by a single Sérsic profile component, with a reduced χ^2 of 1.310. The B_W-band morphology is round rather than elongated. The strong Lyα emission line lies within the B_W filter at a redshift of 2.78. We therefore interpret the diffuse B_W morphology as being likely due to a diffuse Lyα halo around J1432+3358 (cf. Steidel et al. 2011). The Lyα photons from the central galaxy are scattered by the neutral hydrogen gas in the galaxy's circumgalactic medium and form the diffuse Lyα halo. We do not carry out the fitting on the U- and Y-band images because their S/N is too low.

3.3. Spectroscopy

Figure 3 shows the high S/N rest-frame UV spectrum of J1432+3358 taken using the Gemini GMOS-N. The spectrum covers the rest-frame wavelength from 1100 to 1700 Å, and shows the strong Lyα emission line and a few absorption features from the interstellar medium (ISM; e.g., Si II, O I, Si IV, and C IV). In the spectrum, there is no prominent N V 1240 emission line detected at the level of an equivalent width of 2 Å (1σ level) corresponding to a rest-frame equivalent width (EW_0) of 0.5 Å,

Table 2
Lyα Emission and Strong Interstellar Absorption Lines

Line	λ_{rest}[a] (Å)	λ_{obs} (Å)	EW (Å)	FWHM (km s^{-1})	Redshift	Δv[b] (km s^{-1})
Lyα[c]	1215.08	4592.99 ± 0.59	34.97 ± 2.74	1431 ± 81	2.780 ± 0.000	392 ± 38
Lyα(*a*)[d]	1215.08	4597.41[e]	27.46 ± 2.59	852 ± 56	2.784	680
Lyα(*b*)[f]	1215.08	4582.52[e]	9.86 ± 1.38	1073 ± 151	2.771	−291
Lyα(*c*)[g]	1215.08	4601.05 ± 0.36	4.5 ± 1.5	200 ± 25	2.787	923 ± 25
Si II	1259.83	4752.42 ± 1.83	−1.89 ± 0.52	1004 ± 288	2.772 ± 0.001	−222 ± 115
O I	1302.69	4912.05 ± 4.33	−2.65 ± 0.89	2031 ± 643	2.771 ± 0.003	−346 ± 264
Si IV	1393.18	5274.68 ± 2.00	−2.11 ± 0.50	1041 ± 259	2.786 ± 0.001	872 ± 113
C IV	1548.91	5825.82 ± 2.41	−4.04 ± 0.83	1901 ± 384	2.761 ± 0.002	−1101 ± 123

Notes.
[a] Air wavelengths.
[b] The line velocity relative to the systemic redshift. The negative (positive) values correspond to blueshift (redshift).
[c] The whole Lyα emission.
[d] The primary peak of the Lyα emission corresponding to component "a" in Figure 2.
[e] To deblend the two peaks of the Lyα emission line, the central wavelength values are set to the peak values of these two lines and fixed during the fitting.
[f] The secondary peak of the Lyα emission corresponding to component "b" in Figure 2.
[g] The Lyα emission from the faint component corresponding to component "c" in Figure 2. The information of this component is derived from Extractor measurement and Gaussian fitting in the 2D spectra image.

which is much smaller than the EW_0 of 18 ± 10 Å measured in a sample of bright quasars (Forster et al. 2001). Similarly, the C IV 1548, 1551 doublet line shows an absorption rather than emission feature.

J1432+3358 is not detected at the X-ray energies (0.5–7.0 keV) with 30 ks *Chandra* observation (PI: Murray ObsID 13134; see also Murray et al. 2005). The flux limit of the X-ray data is about 4×10^{-16} erg cm^{-2} s^{-1}. By assuming the X-ray spectrum as a common active galactic nucleus (AGN) power-law spectrum with a photon index $\Gamma = 1.7$ (e.g., Kenter et al. 2005), a Galactic neutral hydrogen column density $N_H = 1 \times 10^{20}$ cm^{-2} (e.g., Dickey & Lockman 1990), and an X-ray-to-optical power-law slope $\alpha_{ox} = -1.45$ (e.g., Just et al. 2007), we find that less than 10% of the optical radiation could be from the AGN. J1432+3358 is not detected at 20 cm in the radio wavelength (de Vries et al. 2002), with 1σ sensitivity limit of 28 μJy corresponding to a specific luminosity of 4.7×10^{30} erg s^{-1} Hz^{-1}. This radio limit cannot put a good constraint on the AGN activity in J1432+3358 by adopting the relation between optical and radio luminosity derived from the SDSS quasar sample (White et al. 2007). The rest-frame NIR excess does not show in the *Spitzer* bands, which suggests the absence of hot dust and obscured AGN. The IRAC [3.6]−[4.5] and [5.8]−[8.0] colors are located out of the AGN selection area in MIR color–color space (e.g., Lacy et al. 2004; Stern et al. 2005). The rest-frame UV spectrum, and the non-detection in X-ray and radio bands and MIR colors imply that there is only weak or no AGN (<10%) in J1432+3358, and therefore we suggest that the UV emission is dominated by the emission from massive stars rather than a central AGN.

The properties of the well-detected (S/N > 3) lines in the rest-frame UV spectrum are listed in Table 2. Because the observed wavelength of Lyα emission and ISM absorption lines are affected by galactic-scale outflows, the redshifts from these lines do not represent the systemic redshift (e.g., Adelberger et al. 2005). Typically, the systemic redshift can be derived from absorption lines that are clearly associated with photospheric features (e.g., S V 1502, C III 1176, O VI 1343, etc.; Dey et al. 1997; Shapley et al. 2003), but we cannot identify these lines from the spectrum at the current S/N level. Therefore, we follow Adelberger et al. (2005), in which the redshifts of the Lyα and ISM absorption lines are calibrated with the Hα nebular line in a sample of $z \sim 2$–3 LBGs (see details in Adelberger et al. 2005). The scattering of this relation is less than 0.0015. Here, the systemic redshift of J1432+3358 is estimated from the Lyα and absorption lines using Equations (1) and (2) in Steidel et al. (2010), which are 2.7745 and 2.7755, respectively. This result is also consistent with the systemic redshift calculated using Equation (3) in Adelberger et al. (2005). The systemic redshift of 2.775 ± 0.001 is adopted for further analysis in this paper.

The composite spectrum of LBGs at $z = 2$–3 is also shown in Figure 3 for comparison (Shapley et al. 2003). The continuum shape of the spectrum is similar to that of LBG composite spectrum, indicating that the dust extinction in J1432+3358 is similar to the dust extinction in the typical LBGs. This property is also supported by the spectral energy distribution (SED) fitting results (see details in Section 3.4).

The prominent Lyα emission line is shown in Figures 2 and 3, with an EW_0 of 35 Å. In Figure 2, the Lyα emission shows two peaks separated by 970 km s^{-1} and the FWHM of the Lyα emission line is ∼1500 km s^{-1}, which is much larger than the FWHM(Lyα) = 450 ± 150 km s^{-1} typically found in $z \sim 3$ LBGs (Shapley et al. 2003). The secondary peak is real rather than noise because the double-hump profile is exhibited in the individual spectra of the eight individual 30 minute exposures. Two Gaussian profiles are used to deblend the Lyα emission lines. The FWHMs of the two Lyα components are ∼1000 km s^{-1}. Like most of the LBGs with multiply peaked Lyα emission (Kulas et al. 2012), J1432+3358 shows stronger redshifted Lyα emission than blueshifted. The separation of the two Lyα peaks is ∼1000 km s^{-1}, which is comparable to the separation in other multiple-peaked LBGs (Kulas et al. 2012). Such a Lyα line profile is observed in the expansion shell model (Verhamme et al. 2006), which predicts that a primary Lyα peak is redshifted by approximately two times the expansion velocity and another blueshifted Lyα emission is located around the expansion velocity.

In the two-dimensional (2D) spectral image of the Lyα emission (Figure 2), there are three significant components of Lyα emission detected. The "a" and "b" components that are

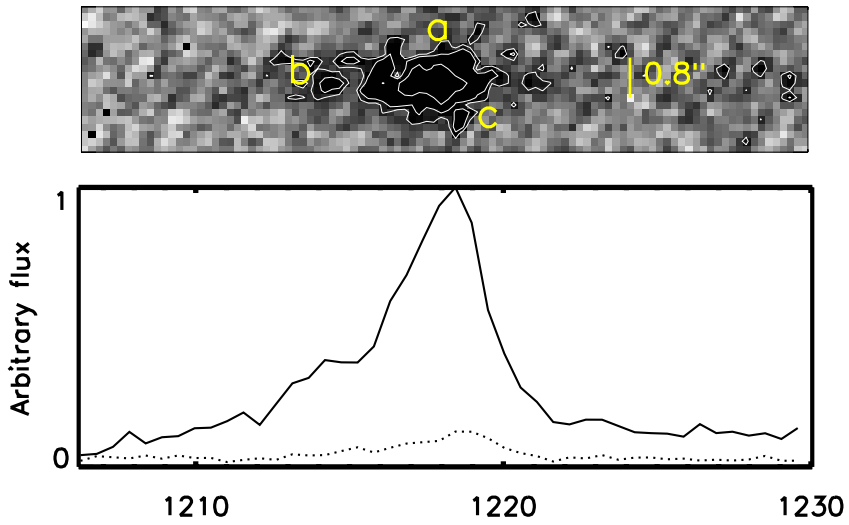

Figure 2. 2D spectrum (top panel) and the 1D spectrum (top panel) of the Lyα emission line. There are three significant components resolved in 2D spectrum image. Components "a" and "b" correspond to the redshifted stronger peak and the blueshifted weaker peak, respectively. Component "c" corresponds to the Lyα emission from the fainter component which was resolved in z-band image. The central wavelength difference between components "a" and "c" is about 3.6 Å.

(A color version of this figure is available in the online journal.)

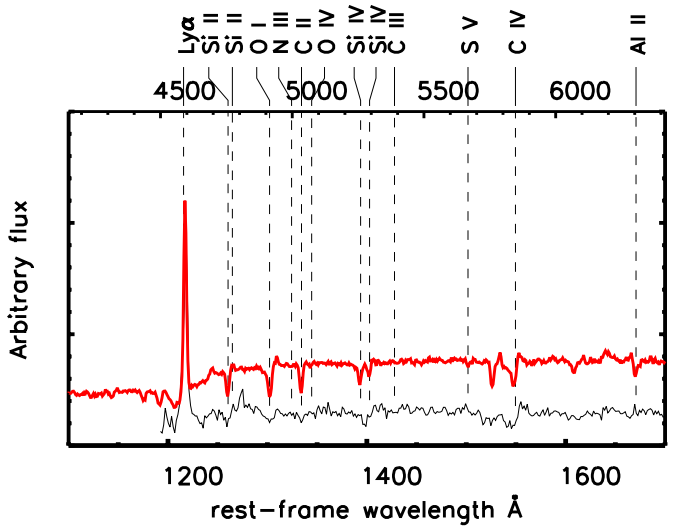

Figure 3. Rest-frame UV spectrum of J1432+3358 in the wavelength range 1100–1700 Å (the thin black solid curve). For comparison, the composite spectrum of a sample of $z \sim 3$ LBGs is also shown with a red thick solid curve (Shapley et al. 2003). The top x-axis represents the observed-frame wavelength. Both spectra are scaled by the peak value of the Lyα emission line, and the composite spectrum is shifted by +0.1 in flux density direction for clarity.

(A color version of this figure is available in the online journal.)

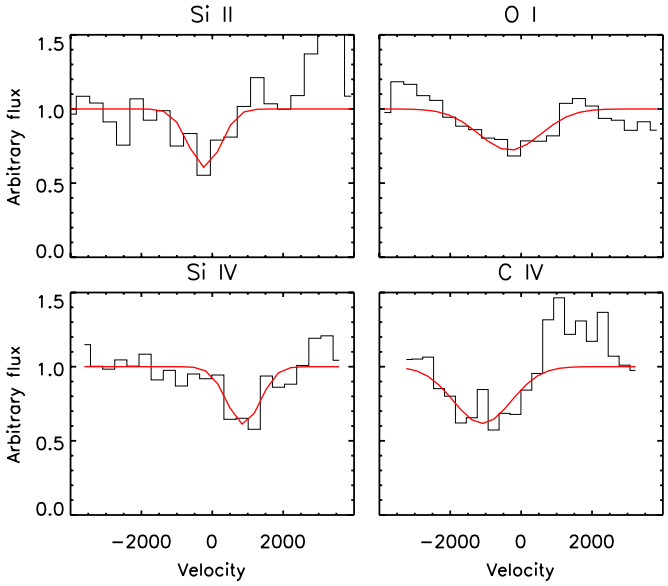

Figure 4. Spectra around the absorption lines (the back curves in histogram mode) and best-fit Gaussian models (the red curves). The flux is scaled by the continuum flux.

(A color version of this figure is available in the online journal.)

resolved in the wavelength direction correspond to the double-peaked feature in the one-dimensional (1D) spectrum. The "c" component resolved in the slit (spatial) direction is the Lyα emission from the fainter component detected in the z-band image. To determine the wavelength of the "c" component, SExtractor and GALFIT are used to obtain the centroid and Gaussian fitting central positions of the "a" and "c" components. The offsets of the central wavelength between the "a" and "c" components are 3.90 Å and 3.25 Å from the measurements with the above two methods, respectively. We adopt 3.64 ± 0.36 as the offset of the central wavelength between the "a" and "c" components, which corresponds to a velocity difference of 237 ± 23 km s^{-1}. The Lyα flux ratio between the components "a" and "c" is about 7:1 from the SExtractor measurement, which is higher than the continuum flux ratio between these two components. The velocity offset and the difference in the flux ratio of Lyα and continuum in components of "a" and "c" also support that J1432+3358 is not a lensed system.

The spectrum also shows that weak absorption lines originated from the ISM, which are Si II, O I, Si IV, and C IV lines (Figure 4). The EW_0 of these absorption features are a few Å, comparable to those in typical LBGs. However, the FWHMs of these lines are 1000 km s^{-1} or even larger (Table 2), about two times larger than those in typical LBGs. The absorption lines show blueshifts with velocities of 200–1000 km s^{-1}, which can be interpreted by a galactic-scale outflow model (Heckman et al. 2000; Steidel et al. 2010). The average outflows velocity estimated from Si II, O I, and C IV absorption lines is -556 ± 103 km s^{-1}. We do not use the Si IV 1392 absorption

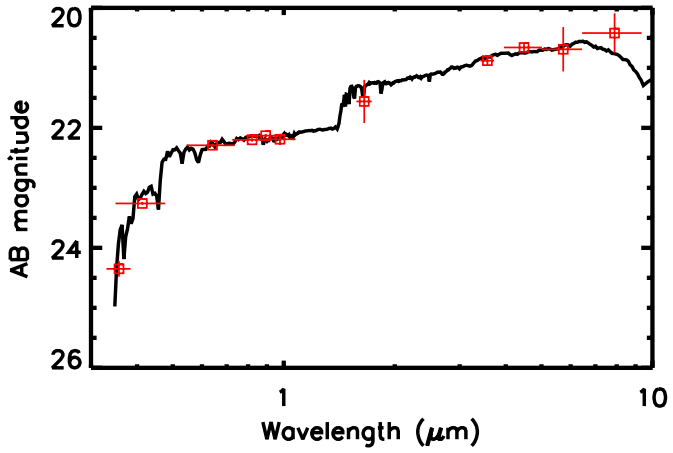

Figure 5. Best-fit stellar synthesis model (solid curve) and photometric data points from *U*-band to IRAC4-band (red squares).

(A color version of this figure is available in the online journal.)

line for the analysis, because the measurements of this line are contaminated by the S IV 1402. Steidel et al. (2010) find that the average outflow velocity LBGs derived from the ISM absorption lines are 164 ± 16 km s^{-1} with a wide range distribution from 0 to 500 km s^{-1}, and we find that the outflow velocities in J1432+3358 are larger than the outflow velocities in most (>98%) LBGs.

3.4. Physical Properties

An IDL-based code Fitting and Assessment of Synthetic Templates (FAST; Kriek et al. 2009) is used to fit the broadband (*U*, B_W, *R*, *I*, *Y*, *H*, IRAC1, IRAC2, IRAC3, and IRAC4) photometry with stellar population synthesis models (Bruzual & Charlot 2003, BC03) and to derive the physical properties of J1432+3358. First, we use an exponential star formation rate (SFR $\propto \exp(-t_{sf}/\tau)$) with a Salpeter initial mass function (Salpeter 1955) and solar metallicity. We adopt the dust extinction law proposed by Calzetti et al. (2000) and the intergalactic medium (IGM) absorption model in Madau (1995). From the SED fitting, we place constraints on the exponential star formation timescale, $\log(\tau(\mathrm{yr})) = 10.00^{+1.00}_{-1.66}$. The large τ value indicates that the SFR declines slowly, suggesting that J1432+3358 has a continuous constant star formation history. Therefore, we adopt a constant star formation history model for further analysis. In Figure 5, we show the best-fit SED overlaid on the optical (*U*, B_W, *R*, and *I*, Y), NIR (*H*), and MIR (IRAC1 (3.6 μm), 2 (4.5 μm), 3 (5.8 μm), 4 (8.0 μm)) photometry. From the fitting, we find that the galaxy age is $\log(t_{sf}(\mathrm{yr})) = 8.8^{+0.2}_{-0.2}$, the SFR is $280^{+70}_{-60}\ M_\odot$ yr^{-1}, the dust extinction is $E(B-V) = 0.12 \pm 0.02$, and the stellar mass is $(1.3 \pm 0.3) \times 10^{11}\ M_\odot$. The SFR derived from the dust-corrected UV luminosity is $310\ M_\odot$ yr^{-1} (Kennicutt 1998a), which is consistent with that derived from the SED fitting. The SFR in J1432+3358 is thus one order of magnitude higher than that in typical $z \sim 3$ LBGs (Shapley et al. 2001). The SED fitting suggests that the star formation age (t_{sf}) is about two times longer than the median star formation time in a typical $z \sim 3$ LBG sample (Shapley et al. 2001). This age is also longer than the typical timescale of the starburst in submillimeter galaxies (SMGs), which is about 200 Myr (e.g., Narayanan et al. 2010). The star formation history and high stellar mass (about 10 times higher than the median stellar mass in a typical $z \sim 3$ LBG sample; Shapley et al. 2001) in J1432+3358 indicate that it is a massive system with a long-term intensive star formation process rather than a low massive system that harbors a star formation burst. However, the physical properties derived from SED fitting are not reliable due to the weak constraints on the star formation timescale (τ). The star formation ages t_{sf} have significant degeneracies with the τ values (see details in Shapley et al. 2001, 2005), which could affect our above conclusion. On the other hand, the stellar mass estimation is much more reliable because the rest-frame NIR *M/L* is reasonably constrained by the SED fitting and nearly independent of the τ values.

The gas mass can be estimated using the global Kennicutt–Schmidt law (Kennicutt 1998b):

$$\Sigma_{\mathrm{gas}} = 361 \times \left(\frac{\Sigma_{\mathrm{SFR}}}{1\ M_\odot\ \mathrm{yr}^{-1}\ \mathrm{kpc}^{-2}}\right)^{0.71} M_\odot\ \mathrm{kpc}^{-2}, \quad (2)$$

where $\Sigma_{\mathrm{SFR}} = \mathrm{SFR}/r_e^2$ and the gas mass, M_{gas}, can be derived from $\Sigma_{\mathrm{gas}} \times r_e^2$, which is $3.7 \times 10^{10}\ M_\odot$. The fraction of gas in J1432+3358, $M_{\mathrm{gas}}/(M_{\mathrm{gas}} + M_{\mathrm{stellar}})$, is 0.2. The low gas fraction is consistent with the gas fraction in the UV-selected galaxies at the most massive end (Erb et al. 2006a) and comparable to that in submillimeter galaxies (Tacconi et al. 2008).

4. DISCUSSION

J1432+3358 shows unique properties compared to normal LBGs, characterized by (1) a high SFR (about 300 $M_\odot$ yr^{-1}), (2) a 3:1 merger-like morphology with a 1.″0 separation of the two components, (3) a high stellar mass ($1.3 \times 10^{11}\ M_\odot$), and (4) a long continuous star formation history (630 Myr), which is two times longer than the median star formation history of LBGs.

One of the key questions regards the nature of UV ultra-luminous LBGs. By integrating the UV luminosity function (e.g., Reddy & Steidel 2009), we find that the space number density of the UV ultra-luminous LBGs with $L > 7L^*$ is a few 10^{-7} Mpc^{-3} in the redshift range from 2.7 to 3.3, which corresponds to a spatial number density of $\sim$0.3 deg^{-2}. This is consistent with the result that there is only one UV ultra-luminous LBG found in the 9 deg^2 NDWFS Boötes field within uncertainties. The space number density of UV ultra-luminous LBGs is about 2–3 orders of magnitude smaller than that of typical star-forming galaxies (e.g., LBGs, Bzk galaxies) at $z \sim 2$–3, which is about 10^{-4}–10^{-5} Mpc^{-3} (e.g., Reddy et al. 2005). On the other hand, the space density of the galaxy with its stellar mass greater than $10^{11}\ M_\odot$ is about 10^{-4} Mpc^{-3}, based on the stellar mass function (e.g., Drory et al. 2005). The low space density of UV ultra-luminous LBGs can be interpreted by the following two different scenarios: the first one is that UV ultra-luminous LBGs can only be found in a short evolutionary phase for the most intensive star-forming galaxies. Although the SED-fitting result shows that the star formation time (t_{sf}) in J1432+3358 is 630 Myr, this galaxy may only be selected by UV-selection method during a short time period, i.e., most of the time the galaxy is highly obscured by dust. The other interpretation is that most of the galaxies that form stars at high intensity are dusty and highly obscured, e.g., SMGs (Chapman et al. 2005) or dust-obscured galaxies (DOGs; Dey et al. 2008; Fiore et al. 2008), and only the small fraction of galaxies that show high SFR are unobscured by dust.

Another crucial question is whether the extremely high SFR in J1432+3358 is triggered by galaxy major mergers or fueled by rapid accretion of cold gas from the IGM. Hopkins et al. (2008)

investigate the role of mergers in the evolution of starburst and quasars and suggest an evolution track from a "typical" galaxy to a gas-rich major merger (see a schematic outline in Figure 1 in Hopkins et al. 2008). In this scenario, at the early stage of merger, i.e., their phase (c), the two interacting galaxies are within one halo but still well separated and can be identified as a merger pair (e.g., Lotz et al. 2004). In this stage, the SFR starts to increase to about 100 $M_{\odot}$ yr^{-1} due to the tidal torques, but the enhanced effect of the SFR is relatively weak compared to the latter coalescence phase. The timescale of this phase is about several million years. The AGN activity in this phase is relatively low. These features are consistent with the properties of J1432+3358.

A tight correlation between the stellar mass ($M_{\rm stellar}$) and SFR (main sequence) in normal star-forming galaxies has been found in both the local and high-redshift universe (e.g., Daddi et al. 2007). The mean value of the specific SFR (sSFR = SFR/$M_{\rm stellar}$) is about 1.8×10^{-9} yr^{-1} in star-forming galaxies at $z \sim 2$ at the high stellar mass end ($10^{11.0}\,M_{\odot} < M_{\rm stellar} < 10^{11.5}\,M_{\odot}$). Galaxies with sSFR greater than $\sim 5.6 \times 10^{-9}$ yr^{-1} are considered to be off the main sequence and suggested to be merger-driven starburst galaxies (e.g., Rodighiero et al. 2011). The sSFR of J1432+3358 is 1.9×10^{-9} yr^{-1}, which would locate our galaxy right on the galaxy main sequence at $z \sim 2$. This result implies that the SFR in J1432+3359 is not enhanced by the merger process, which is also consistent with this system being in the early phase of the merger process. However, the above conclusion is based on the SED fitting results, which are subject to large systematic uncertainty as discussed in Section 3.3. Therefore, further high-resolution space-based imaging and ground-based integral field unit (IFU) observations will be requested to provide more firm evidence to determine whether J1432+3358 is a major merger or a clumpy disk galaxy.

The outflow properties of J1432+3358 can be studied and compared to the typical LBGs. Steidel et al. (2010) do not find a correlation between the SFR and the velocity of the wind in the UV-selected galaxies at $z \sim 2$, which is found in other high-redshift galaxies (Weiner et al. 2009). One interpretation is that the SFR dynamic range in the Steidel et al. (2010) sample is too small to reveal the relation. With the SFR an order of magnitude higher than for typical $z \sim 2$ UV-selected galaxies, J1432+3358 will provide enough dynamic range to check whether a correlation exists between the SFR and outflow velocity. Comparing J1432+3358 to the typical $z \sim 2$ UV-selected galaxies (Steidel et al. 2010), we do find that the outflow velocity increases with SFR, and roughly follows the relation found in Weiner et al. (2009), $v_{\rm out} \propto {\rm SFR}^{0.3}$.

We thank the anonymous referee for providing constructive comments and help in improving the manuscript. This work made use of images and/or data products provided by the NOAO Deep Wide-Field Survey (Jannuzi & Dey 1999, which is supported by the National Optical Astronomy Observatory, NOAO). NOAO is operated by AURA, Inc., under a cooperative agreement with the National Science Foundation. We thank the LBTO, NOAO, and Gemini staff for their great support in preparing the observing and carrying out the observing. F.B. thanks M. Kriek for providing her IDL SED-fitting package and C. Peng for discussion on GALFIT. Y.T.L. is grateful to the HyperSuprimeCam software development team for the aid of reduction of the SuprimeCam data. F.B., X.F., L.J., and I.M. acknowledge support from a Packard Fellowship for Science and Engineering and NSF grant AST 08-06861.

Facilities: LBT, MMT, Gemini:Gillett, Mayall, *Spitzer*, Subaru

REFERENCES

Adelberger, K. L., Shapley, A. E., Steidel, C. C., et al. 2005, ApJ, 629, 636
Adelberger, K. L., Steidel, C. C., Giavalisco, M., et al. 1998, ApJ, 505, 18
Allam, S. S., Tucker, D. L., Lin, H., et al. 2007, ApJ, 662, L51
Ashby, M. L. N., Stern, D., Brodwin, M., et al. 2009, ApJ, 701, 428
Bentz, M. C., Pogge, R. W., & Osmer, P. S. 2008, AJ, 136, 498
Bertin, E., & Arnouts, S. 1996, A&AS, 117, 393
Bouwens, R. J., Illingworth, G. D., Franx, M., & Ford, H. 2008, ApJ, 686, 230
Bouwens, R. J., Illingworth, G. D., Labbe, I., et al. 2011, Nature, 469, 504
Bruzual, G., & Charlot, S. 2003, MNRAS, 344, 1000
Calzetti, D., Armus, L., Bohlin, R. C., et al. 2000, ApJ, 533, 682
Chapman, S. C., Blain, A. W., Smail, I., & Ivison, R. J. 2005, ApJ, 622, 772
Cooke, J., Barton, E. J., Bullock, J. S., Stewart, K. R., & Wolfe, A. M. 2008, ApJ, 681, L57
Cowie, L. L., Songaila, A., Hu, E. M., & Cohen, J. G. 1996, AJ, 112, 839
Daddi, E., Dickinson, M., Morrison, G., et al. 2007, ApJ, 670, 156
de Vries, W. H., Morganti, R., Röttgering, H. J. A., et al. 2002, AJ, 123, 1784
Dey, A., Soifer, B. T., Desai, V., et al. 2008, ApJ, 677, 943
Dey, A., van Breugel, W., Vacca, W. D., & Antonucci, R. 1997, ApJ, 490, 698
Dickey, J. M., & Lockman, F. J. 1990, ARA&A, 28, 215
Diehl, H. T., Allam, S. S., Annis, J., et al. 2009, ApJ, 707, 686
Drory, N., Salvato, M., Gabasch, A., et al. 2005, ApJ, 619, L131
Erb, D. K., Shapley, A. E., Pettini, M., et al. 2006a, ApJ, 644, 813
Erb, D. K., Steidel, C. C., Shapley, A. E., et al. 2006b, ApJ, 647, 128
Ferguson, H. C., Dickinson, M., Giavalisco, M., et al. 2004, ApJ, 600, L107
Fiore, F., Grazian, A., Santini, P., et al. 2008, ApJ, 672, 94
Forster, K., Green, P. J., Aldcroft, T. L., et al. 2001, ApJS, 134, 35
Giallongo, E., Ragazzoni, R., Grazian, A., et al. 2008, A&A, 482, 349
Giavalisco, M. 1998, in The Hubble Deep Field, ed. M. Livio, S. M. Fall, & P. Madau (New York: Cambridge Univ. Press), 121
Giavalisco, M., Steidel, C. C., Adelberger, K. L., et al. 1998, ApJ, 503, 543
Heckman, T. M., Lehnert, M. D., Strickland, D. K., & Armus, L. 2000, ApJS, 129, 493
Hill, J. M., Green, R. F., Ashby, D. S., et al. 2010, Proc. SPIE, 7733, 10
Hopkins, P. F., Hernquist, L., Cox, T. J., & Kereš, D. 2008, ApJS, 175, 356
Jain, B., & Lima, M. 2011, MNRAS, 411, 2113
Jannuzi, B. T., & Dey, A. 1999, in ASP Conf. Ser. 191, Photometric Redshifts and the Detection of High Redshift Galaxies, ed. R. Weymann, L. Storrie-Lombardi, M. Sawicki, & R. Brunner (San Francisco, CA: ASP), 111
Just, D. W., Brandt, W. N., Shemmer, O., et al. 2007, ApJ, 665, 1004
Kennicutt, R. C., Jr. 1998a, ARA&A, 36, 189
Kennicutt, R. C., Jr. 1998b, ApJ, 498, 541
Kenter, A., Murray, S. S., Forman, W. R., et al. 2005, ApJS, 161, 9
Kriek, M., van Dokkum, P. G., Labbé, I., et al. 2009, ApJ, 700, 221
Kulas, K. R., Shapley, A. E., Kollmeier, J. A., et al. 2012, ApJ, 745, 33
Lacy, M., Storrie-Lombardi, L. J., Sajina, A., et al. 2004, ApJS, 154, 166
Lee, K.-S., Giavalisco, M., Conroy, C., et al. 2009, ApJ, 695, 368
Lee, K.-S., Giavalisco, M., Gnedin, O. Y., et al. 2006, ApJ, 642, 63
Lilly, S. J., Le Fevre, O., Hammer, F., & Crampton, D. 1996, ApJ, 460, L1
Lin, H., Buckley-Geer, E., Allam, S. S., et al. 2009, ApJ, 699, 1242
Lotz, J. M., Primack, J., & Madau, P. 2004, AJ, 128, 163
Madau, P. 1995, ApJ, 441, 18
Madau, P., Ferguson, H. C., Dickinson, M. E., et al. 1996, MNRAS, 283, 1388
Mehlert, D., Seitz, S., Saglia, R. P., et al. 2001, A&A, 379, 96
Murray, S. S., Kenter, A., Forman, W. R., et al. 2005, ApJS, 161, 1
Narayanan, D., Hayward, C. C., Cox, T. J., et al. 2010, MNRAS, 401, 1613
Peng, C. Y., Ho, L. C., Impey, C. D., & Rix, H.-W. 2002, AJ, 124, 266
Reddy, N. A., Erb, D. K., Steidel, C. C., et al. 2005, ApJ, 633, 748
Reddy, N. A., & Steidel, C. C. 2009, ApJ, 692, 778
Rodighiero, G., Daddi, E., Baronchelli, I., et al. 2011, ApJ, 739, L40
Salpeter, E. E. 1955, ApJ, 121, 161
Sand, D. J., Treu, T., Ellis, R. S., & Smith, G. P. 2005, ApJ, 627, 32
Sérsic, J. L. 1963, Bol. Asociacion Argentina Astron. La Plata Argentina, 6, 41
Shapley, A. E., Steidel, C. C., Adelberger, K. L., et al. 2001, ApJ, 562, 95
Shapley, A. E., Steidel, C. C., Erb, D. K., et al. 2005, ApJ, 626, 698
Shapley, A. E., Steidel, C. C., Pettini, M., & Adelberger, K. L. 2003, ApJ, 588, 65
Smail, I., Swinbank, A. M., Richard, J., et al. 2007, ApJ, 654, L33
Spergel, D. N., Bean, R., Doré, O., et al. 2007, ApJS, 170, 377
Steidel, C. C., Adelberger, K. L., Shapley, A. E., et al. 2003, ApJ, 592, 728
Steidel, C. C., Bogosavljević, M., Shapley, A. E., et al. 2011, ApJ, 736, 160

Steidel, C. C., Erb, D. K., Shapley, A. E., et al. 2010, ApJ, 717, 289
Steidel, C. C., Giavalisco, M., Pettini, M., Dickinson, M., & Adelberger, K. L. 1996, ApJ, 462, L17
Steidel, C. C., Shapley, A. E., Pettini, M., et al. 2004, ApJ, 604, 534
Stern, D., Eisenhardt, P., Gorjian, V., et al. 2005, ApJ, 631, 163
Tacconi, L. J., Genzel, R., Smail, I., et al. 2008, ApJ, 680, 246
Turner, E. L., Ostriker, J. P., & Gott, J. R., III 1984, ApJ, 284, 1
van der Burg, R. F. J., Hildebrandt, H., & Erben, T. 2010, A&A, 523, A74
Verhamme, A., Schaerer, D., & Maselli, A. 2006, A&A, 460, 397
Weiner, B. J., Coil, A. L., Prochaska, J. X., et al. 2009, ApJ, 692, 187
White, R. L., Helfand, D. J., Becker, R. H., Glikman, E., & de Vries, W. 2007, ApJ, 654, 99